Biomacromolecules

ARTICLE

pubs.acs.org/Biomac

Modifying the Body Distribution of HPMA-Based Copolymers by Molecular Weight and Aggregate Formation

Mareli Allmeroth,[†,#] Dorothea Moderegger,[‡,#] Barbara Biesalski,[§] Kaloian Koynov,[⊥] Frank Rösch,[‡] Oliver Thews,[∥] and Rudolf Zentel*[,†]

[†]Institute of Organic Chemistry, Johannes Gutenberg University, Duesbergweg 10-14, 55099 Mainz, Germany

[‡]Institute of Nuclear Chemistry, Johannes Gutenberg University, Fritz-Strassmann-Weg 2, 55128 Mainz, Germany

[§]Institute of Physiology and Pathophysiology, University Medicine Mainz, Duesbergweg 6, 55128 Mainz, Germany

[∥]Institute of Physiology, University Halle, Magdeburger Str. 6, 06097 Halle (Saale), Germany

[⊥]Max-Planck-Institute for Polymer Research, Ackermannweg 10, D-55128 Mainz, Germany

Supporting Information

ABSTRACT: There is a recognized need to create well-defined polymer probes for in vivo and clinical positron emission tomography (PET) imaging to guide the development of new generation polymer therapeutics. Using the RAFT polymerization technique in combination with the reactive ester approach, here we have synthesized well-defined and narrowly distributed *N*-(2-hydroxypropyl)methacrylamide homopolymers (pHPMA) (**P1*** and **P2***) and random HPMA copolymers consisting of hydrophilic HPMA and hydrophobic lauryl methacrylate comonomers (**P3*** and **P4***). The polymers had molecular weights below (**P1*** and **P3***) and above the renal threshold (**P2*** and **P4***). Whereas the homopolymers dissolve in isotonic solution as individual coils, the random copolymers form larger aggregates above their critical micelle concentration (~40 nm), as determined by fluorescence correlation spectroscopy. Structure−property relationships of the pharmacokinetics and biodistribution of the different polymer architectures were monitored in the living organism following radiolabeling with the positron emitter ^{18}F via fluoroethylation within a few hours. Ex vivo organ biodistribution and in vivo μPET imaging studies in male Copenhagen rats revealed that both size and the nature of the aggregate formation (hydrophobically modified copolymers) played a major role in blood clearance and biodistribution, especially concerning liver and kidney accumulation. The high-molecular-weight random copolymer **P4*** (hydrophobically modified), in particular, combines low liver uptake with enhanced blood circulation properties, showing the potential of hydrophobic interactions, as seen for the represented model system, that are valuable for future drug carrier design.

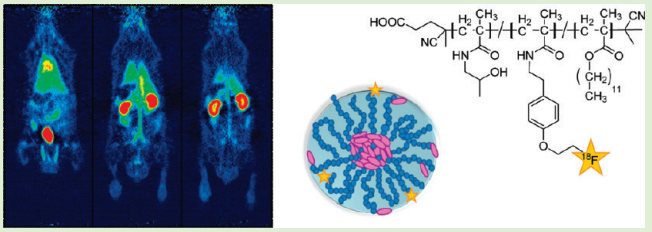

1. INTRODUCTION

"Polymer therapeutics", a term describing polymeric drugs, polymer−drug conjugates, polymer−protein conjugates, polymeric micelles, and polyplexes, became an emerging field of interest in both chemical and medical sciences over the last four decades.[1] Their diversity regarding loading capacity with multiple pharmaceutics, reduction of usually occurring toxic side effects, as well as an inherent tendency to accumulate in tumor tissue due to the EPR (enhanced permeability and retention) effect,[2,3] constitutes them as an attractive tool for clinical applications. On the basis of the first concept of Ringsdorf in the 1970s,[4] concerning a macromolecular-based drug delivery vehicle for active and passive targeting for improving the therapeutic action, fundamental research in this discipline has evolved. Intensive studies on polymer−drug conjugates,[5−9] micelle-forming polymers,[10−13] or newly established polymer−enzyme combination therapy[14−16] have been carried out, demonstrating the great potential of the route pursued. Altogether, only poly(ethylene glycol) (PEG), poly-*N*-(2-hydroxypropyl)-methacrylamide) (HPMA) copolymers, dextran derivatives, as well as polyglutamic-acid-based drug conjugates have progressed into clinical trials, six among them being HPMA anticancer conjugates.[1,9,17]

Regarding the clinical application of polymer-based therapeutics, there is a need for appropriate preclinical screening methodologies to select a suitable therapy for the individual patient.[18,19] In this respect, introducing small radioactive probes into the polymeric system and using nuclear medicine imaging techniques such as positron emission tomography (PET), pharmacokinetics, and distribution of the polymer therapeutic can be easily monitored. Depending on the biological time frame to be monitored, PET-nuclide and labeling strategy need to be adjusted. On the basis of the short-lived positron emitter fluorine-18 ($t_{1/2}$ = 110 min), we have recently developed PET-based HPMA copolymers for short-term in vivo visualization, thereby being time-efficient

Received: April 26, 2011
Revised: June 9, 2011
Published: June 14, 2011

and enabling minimal radiation exposure concerning a clinical application.[20] In contrast, also new labeling approaches for HPMA-based polymers using PET-nuclides of longer half-lives, for example, $^{72/74}$As ($t_{1/2}(^{72}\text{As})$ = 26 h, $t_{1/2}(^{74}\text{As})$ = 17.8 days) were established, offering the possibility for long-term PET-imaging with time frames of weeks to months.[21]

By introducing fluorine-18 as PET nuclide, initial excretion pathways and organ uptake can be identified and measured quantitatively. Because of its excellent physical and nuclear characteristics, fluorine-18 is considered to be the ideal radioisotope for PET imaging probes, providing visualization of high spatial resolution, and because of its size, not influencing the polymeric structure. In contrast with radionuclides for SPECT (single photon emission computed tomography) (e.g., ^{123}I, ^{131}I, and ^{99m}Tc), so far used to image HPMA-based polymers,[22,23] fluorine-18 as short-lived isotope combines the requirements for fast and detailed screening of potential drug carrier systems giving insight into individual early phase accumulations and clearance mechanisms.

Regarding the therapeutic effects of a polymer-based drug carrier system, its backbone plays a crucial role. Essential requirements are mainly either biodegradability or biocompatibility with final excretion properties. Being water-soluble, nontoxic, and nonimmunogenic, poly-*N*-(2-hydroxypropyl)methacrylamide) has evolved as a promising biocompatible artificial polymer, already intensively studied in vitro and in vivo.[9,24−26] Compared with PEG, it possesses the advantage of multifunctionality whereas PEG has only two functional end groups. That enables covalent conjugation of a higher drug payload, attachment of recognition units for receptor-mediated targeting, or combination therapy.[15]

When being developed as a polymer therapeutic, it is important that a polymer should be as well-defined as possible.[27] The first HPMA-based polymers were, however, originally made by free radical polymerization[28−31] and required lengthy as well as laborious fractionation processes to reduce their polydispersity.[32] With the introduction of living radical polymerization techniques, well-defined polymer structures became available, either by ATRP or by RAFT techniques.[33−36] Especially in combination with the reactive ester approach,[12,20,37] RAFT offers an elegant access to different polymer architectures and various functional groups; for example, imaging moieties or therapeutics can be attached. By applying this route, HPMA random as well as block copolymers of specific composition can be easily prepared, exhibiting the tendency to aggregate in solution because of hydrophobic laurylmethacrylate side chains.[12]

To be effective as an antitumor agent, a polymer drug conjugate must be able to localize to the tumor tissue by the EPR-effect[2,38] (resulting from leaky tumor blood vessels and a lack of lymphatic drainage) and prevent the drug from localizing to normal tissues that are potential sites of toxicity. Furthermore, long circulation properties in the blood pool might be beneficial for a controlled and continuous drug release.

Lammers et al.[39] applied radiolabeling with SPECT isotope iodine-131 to investigate the influence of the incorporation of various functional groups into HPMA (copolymers) on the body distribution and accumulation in the tumor. This work included polymer therapeutics like PK1 polymers but focused on functional groups that interact by H-bonding or ionic charges like carboxylate, amine groups, or peptides. The authors found that the copolymer units mostly reduced the circulation time in the body but did not change the relative accumulation in different tissues as well as the tumor. Classical polymeric therapeutics like PK1 or PK2[40,41] often carry hydrophobic pharmaceutics. On the basis of these characteristics, they are, in a physicochemical sense, hydrophobically modified copolymers. This underlines the importance of also focusing on the aspect of intra- and intermolecular aggregate formation due to hydrophobic interactions in model systems. In this respect, the synthesis of HPMA-based hydrophilic/hydrophobic copolymers and their aggregate formation makes model systems available in which it is easy to vary the size and the hydrophilic/hydrophobic balance. Experiments with cell cultures already demonstrated the tremendous influence of the variation of these segments on the cellular uptake of HPMA-based polymers,[12] and recent studies underline their potential to transport pharmaceutics across the blood−brain barrier.[42]

Consequently, the aim of the present study focused on the determination of correlations between size and aggregate formation due to hydrophobic interactions and resulting biological properties (body and organ distribution) of well-defined HPMA-based polymers in living animals.

Applying fast and versatile radiolabeling techniques for noninvasive high-resolution PET imaging helps us to understand how the in vivo fate of a polymer model system can be affected by structural modification, thus speeding up the time-consuming evaluation process necessary for the design of potential drug carrier candidates.

2. MATERIALS AND METHODS

2.1. Materials. All solvents were of analytical grade, as obtained by Sigma Aldrich and Acros Organics. Dioxane was distilled over a sodium/potassium composition. Lauryl methacrylate was distilled to remove the stabilizer and stored at −18 °C. 2,2′-Azo-bis-(isobutyronitrile) (AIBN) was recrystallized from diethyl ether and stored at −18 °C as well.

2.2. Characterization. ^{1}H NMR spectra were obtained by a Bruker AC 300 spectrometer at 300 MHz. ^{19}F-NMR analysis was carried out with a Bruker DRX-400 at 400 MHz. All measurements were accomplished at room temperature, and spectroscopic data were analyzed using ACDLabs 9.0 1D NMR manager. The synthesized polymers were dried at 40 °C under vacuum overnight, followed by gel permeation chromatography (GPC). GPC was performed in tetrahydrofuran (THF) as solvent using the following equipment: pump PU 1580, autosampler AS 1555, UV detector UV 1575, and RI detector RI 1530 from Jasco as well as a miniDAWN Tristar light scattering detector from Wyatt. Columns were used from MZ Analysentechnik, 300 × 8.0 mm: MZ-Gel SDplus 10^6 Å 5 μm, MZ-Gel SDplus 10^4 Å 5 μm, and MZ-Gel SDplus 10^2 Å 5 μm. GPC data were evaluated by using the software PSS WinGPC Unity from Polymer Standard Service Mainz. The flow rate was set to 1 mL/min with a temperature of 25 °C.

For synthesis of 2-[^{18}F]fluoroethyl-1-tosylate ([^{18}F]FETos), a Sykam S 1100 pump and a Knauer UV-detector (K-2501) HPLC system were used. Size exclusion chromatography (SEC) of ^{18}F-labeled polymers was performed using HiTrap Desalting Column, Sephadex G-25 Superfine and a waters pump (1500 series), a Waters UV-detector (2487 λ absorbance detector), and a Berthold LB 509 radiodetector.

In ex vivo studies, fluorine-18 activities were determined using a Perkin-Elmer 2470 Wizard^2 γ-counter.

2.3. Synthesis of the Polymers. The polymers **P1*** to **P4*** were prepared by analogy to refs 12 and 20. The details are added as Supporting Information.

2.4. Characterization of the Polymers. The amphiphilic character of the hydrophobically modified HPMA copolymers (P3 and P4) was characterized by a "du Noüy" ring tensiometer used to determine the cmc (critical micelle concentration) in isotonic sodium chloride solution. The protocol can be found as Supporting Information.

Scheme 1. Reaction Scheme of Polymeric Precursor Systems Based on the Reactive Ester Approach and Their Polymer-Analogous Conversion for Further Radioactive Labeling

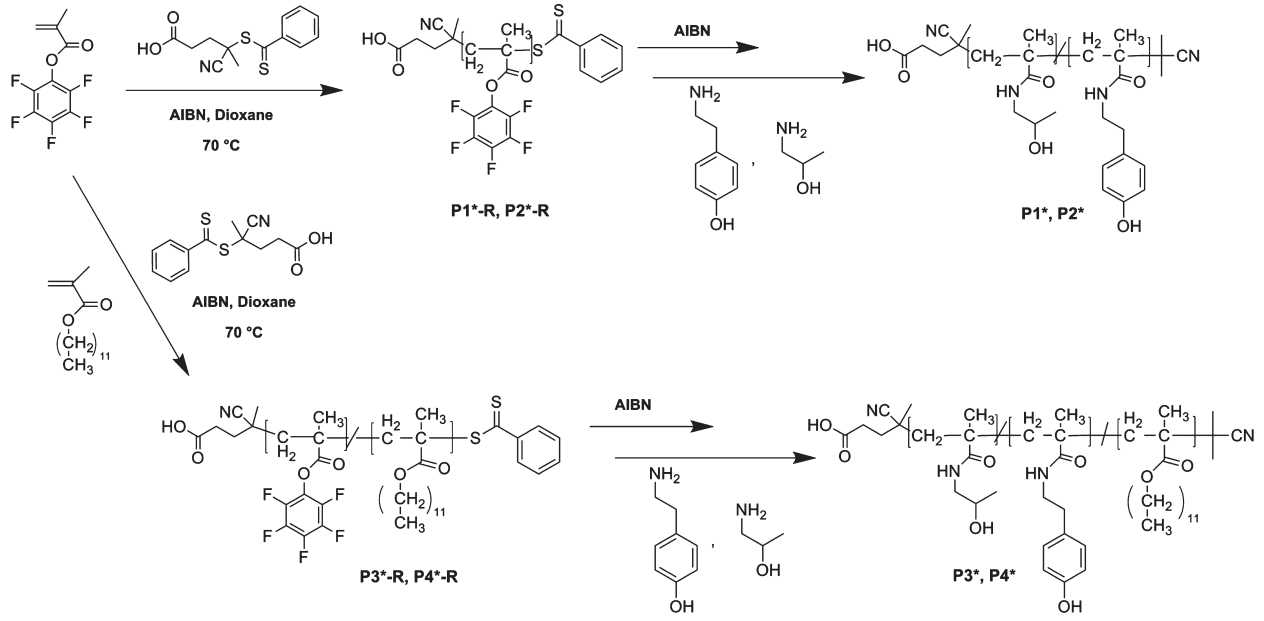

The hydrodynamic radii of the polymeric systems were determined by fluorescence correlation spectroscopy (FCS) using a commercial FCS setup. This method proves the aggregate formation of the copolymers. The details can be found in the Supporting Information.

2.5. Radiolabeling and Purification for Ex Vivo and In Vivo Experiments. Synthesis of [^{18}F]FETos, labeling of polymers **P1***−**P4***, as well as purification of labeled polymers for ex vivo and in vivo experiments was accomplished according to literature.[20]

For metabolic studies, blood samples were taken 140 min p.i. and centrifuged, and blood plasma was analyzed using SEC. Details are provided as Supporting Information.

2.6. Animal Experiments. *2.6.1. Tumor and Animal Model.* Tumor experiments were performed with the subline AT1 R-3327 Dunning prostate carcinoma of the rat. Tumors were used when they reached a volume of 1 to 2 mL ~10 to 14 days after tumor cell injection. At this time point, tumors were in the exponential growing phase and did not show signs of necrosis (confirmed by histology; data not shown). All experiments had previously been approved by the regional animal ethics committee and were conducted in accordance with the German Law for Animal Protection and the UKCCCR Guidelines.[43] Details are provided as Supporting Information.

2.6.2. Biodistribution Measurements. To assess the distribution of the radiolabeled polymers in different organs of the animals, we injected the polymer (concentration of 1 mg in 1 mL sodium chloride solution) i.v. in anaesthetized tumor-bearing rats via the tail vein with a mean activity of 18.7 ± 5.8 MBq. After 120 or 240 min, the animals were sacrificed and different organ (kidney, liver, lung, spleen, heart, skeletal muscle, small intestine, testis, blood) and tumor samples were taken. The tissue samples were weighed and minced. Finally, the ^{18}F-activity in the organs was measured in a γ-counter.

2.6.3. Small Animal PET Studies. In addition, the uptake of the different polymers in tumors and organs was imaged using PET. Details of the imaging procedure are described as Supporting Information.

3. RESULTS AND DISCUSSION

3.1. Synthetic Concept of HPMA Based Homo- and Random Copolymers. To study the in vivo behavior of different polymeric architectures in dependence of their molecular weight and the effect of aggregate formation due to the presence of hydrophobic segments, diverse HPMA-based polymeric systems were synthesized by applying the RAFT polymerization technique.[33,34,44] Barz et al. already found that especially the aggregate formation significantly influences the cellular entry into MCF7/ADR cells in vitro.[12] Here we aimed to gain more knowledge about structure−property relationships not only on the cellular level but also in the living organism. First results emphasized a successful radioactive labeling of such polymers.[20] For further systematic studies, a series of HPMA homopolymers and HPMA-*ran*-LMA copolymers were prepared, with molecular weights chosen to be below and above the renal threshold (limit of renal clearance of HPMA copolymers M_w < 40 000 g/mol[45]). The incorporation of the hydrophobic lauryl methacrylate constitutes the basis for aggregate formation. Because of differences in size and aggregate formation, we expected different pharmacological behavior in terms of organ accumulation, circulation time, as well as excretion characteristics. The synthetic route to these polymers (**P1***−**P4***) is depicted in Scheme 1.

Starting with the pentafluorophenyl methacrylate monomer, the precursor homopolymers **P1*-R** and **P2*-R** were synthesized, and by simultaneous addition of lauryl methacrylate, the random copolymers **P3*-R** and **P4*-R**. The polymerization was achieved according to literature.[12,46,47] These reactive polymers can afterward be converted to HPMA-based polymers by a clean conversion. A main advantage of this synthetic route to HPMA-*ran*-LMA copolymers lies in the random copolymerization of two methacrylate-based monomers (both esters). Because of the comparable copolymerization parameters, a random, nonblocky integration of both monomers is reasonable. (Copolymerization parameters were determined with r_1 and r_2 both <1.) This provides an important advantage compared with the copolymerization of amides with esters.[48] In addition, the primarily formed reactive polymers **P1*-R** to **P4*-R** are well soluble and do not form aggregates because all monomer units are hydrophobic. The dithioester end group was cleaved by an excess of

Table 1. Analytical Data of Reactive Ester Homopolymers (P1*-R, P2*-R) and Random Copolymers (P3*-R, P4*-R) As Well As the Final Polymeric Structures P1*−P4* (See Scheme 1)

nomenclature	polymeric structure	monomer ratio	M_n in g/mol	M_w in g/mol	PDI[b]
P1*-R	homopolymer	100%[a]	18000[b]	23000[b]	1.29
P2*-R	homopolymer	100%[a]	87000[b]	130000[b]	1.49
P3*-R	random copolymer	80:20[a]	17000[b]	21000[b]	1.26
P4*-R	random copolymer	80:20[a]	57000[b]	80000[b]	1.41
P1*	homopolymer	100%[c]	9000[d]	12000[d]	1.29
P2*	homopolymer	100%[c]	52000[d]	77000[d]	1.49
P3*	random copolymer	82:18[c]	11000[d]	14000[d]	1.26
P4*	random copolymer	75:25[c]	39000[d]	55000[d]	1.41

[a] Calculated monomer ratio. [b] Determination by GPC in THF as solvent. [c] Monomer ratio determined by ^{1}H NMR spectroscopy after polymer-analogous reaction with 2-hydroxypropylamine (**P1*−P4***). [d] Calculated from the molecular weights of the reactive ester polymers **P1*-R** to **P4*-R** as determined by GPC in THF as solvent.

2,2′-azo-bis-(isobutyronitrile), a method first presented by Perrier et al.,[49] possessing the benefit of avoiding side reactions during the postpolymerization step. The polymeric precursors were functionalized by aminolysis via tyramine groups, necessary for further radioactive labeling. The incorporation efficiency was calculated to be 2−4% for each polymer chain. 2-Hydroxypropylamine was finally added, resulting in the polymeric structures **P1*−P4***. Full conversion of the reactive ester side groups could be proven by means of ^{19}F-NMR spectroscopy, demonstrating complete disappearance of the ^{19}F-signals at the polymeric backbone.

3.2. Molecular Weights and Incorporation Ratios of Polymeric Architectures. Overall, four different polymeric systems were synthesized (all hydrophilic polymers **P1*** and **P2*** for reference and hydrophilic/hydrophobic copolymers **P3*** and **P4***), each architecture exhibiting a low- and high-molecular-weight sample. Characterization of the precursor structures **P1*-R−P4*-R** was carried out using gel permeation chromatography. The results are summarized in Table 1. As indicated, well-defined polymeric systems with relatively narrow molecular weight distribution have been achieved by the RAFT polymerization process (PDI = 1.26 to 1.49).

3.3. Aggregation Parameter. The major distinction between homo- and copolymers relies in the formation of micelle-like structures due to the incorporation of hydrophobic groups, in our case lauryl methacrylate. To determine the concentration-dependent aggregation behavior of the copolymers **P3*** and **P4***, the cmc was determined by surface tension measurements with a "du Noüy" ring tensiometer. Stock solutions of 0.1 mg/mL in 0.9% NaCl solution were prepared, and the measurement was performed at 37 °C to mimic in vivo conditions. For the low-molecular-weight copolymer **P3***, a cmc value of 4.6×10^{-3} mg/mL was obtained. Copolymer **P4*** exhibited a lower cmc of 1.6×10^{-3} mg/mL, which is reasonable because of the increased LMA ratio. On the basis of these data, it can be assumed that the polymeric aggregates are also present in the bloodstream of the rat (blood volume of the rat ∼16 mL,[50] corresponding to a concentration of 6.3×10^{-2} mg/mL polymer in the blood after intravenous injection of 1 mL of a 1 mg/mL isotonic solution). Even after renal clearance of >50% of the polymer injected, the micellar-like structure should be retained. The cmc values are additionally summarized in Table 2.

To facilitate size determination of the aggregates formed from the amphiphilic copolymers in water, we additionally attached fluorescent Oregon Green 488 cadaverine onto the polymer chains. Fluorescence correlation spectroscopy was used to determine the diffusion constants of the individual polymer chains as well as of the aggregates and hence their hydrodynamic radii. The homopolymer **P1*** exhibited a hydrodynamic radius of 1.1 nm and the higher molecular weight polymer **P2*** exhibited a size of 3 nm (NaCl solution). Both values are a bit smaller than expected (for **P4*** in methanol, as nonaggregating solvent, we observed a hydrodynamic radius of 6 nm) and are just taken as proof for the existence of individual random coils. The random copolymers **P3*** and **P4*** showed a different behavior and a superstructure formation. Copolymer **P3*** possessed a hydrodynamic radius of 33 nm and the random copolymer **P4*** an R_h of ∼40 nm. Both values are much too large for individual chains but also for classical micelles in which the size should not be much larger than two times the size of the individual chain. These data are consistent with previous observations from our group.[12] They may be explained by the formation of "compound micelles".[51] Also, Haag and coworkers reported the formation of unexpectedly large supramolecular assemblies for nonionic dendritic amphiphiles being composed of hydrophilic polyglycerol dendrons and hydrophobic C_{11} or C_{16} alkyl chains.[52] The formation of more complex hydrophobic/hydrophilic superstructures can be the reason for the hydrodynamic radii of the random copolymer superstructures. A collection of the sizes for polymers **P1*−P4*** is given in Table 3.

Table 2. Critical Micelle Concentration of Random Copolymers (P3*, P4*) in Isotonic NaCl Solution at 37°C

nomenclature	polymeric structure	cmc in mg/mL[a]	cmc in mol/L
P3*	random copolymer	4.6×10^{-3}	4.2×10^{-7}
P4*	random copolymer	1.6×10^{-3}	4.2×10^{-8}

[a] As determined by surface tension versus concentration applying the ring method of the "du Noüy" ring tensiometer.

3.4. Radioactive Labeling with [^{18}F]Fluorine. To study the behavior of the different polymeric architectures in vivo, the positron emitter fluorine-18 ($t_{1/2}$ = 109.7 min) was introduced for both ex vivo organ distribution measurements as well as μPET imaging via a prosthetic labeling procedure using [^{18}F]FETos. Compared with γ-imaging using SPECT nuclides (e.g., ^{99m}Tc or ^{123}I), PET provides images of much higher spatial resolution because of the nuclear characteristics of fluorine-18. For labeling purposes, the polymeric backbone had been derivatized with 2−4% of tyramine groups (these groups were present during the experiments

described above), thus offering a reactive site for the regioselective incorporation of the [^{18}F]fluoroethyl moiety.[20] The applied indirect labeling method is shown in Scheme 2. In a first step, fluorine-18 is incorporated via nucleophilic substitution, yielding [^{18}F]FETos and subsequently transferred to a solution of the tyramine-derivatized polymer, which is deprotonated using a small amount of base.

Decay-corrected radiochemical yields (RCYs) were determined by SEC and are summarized in Table 4. RCYs were found to be dependent on the molecular weight and the lauryl methacrylate ratio at constant temperature. RCYs for the low-molecular-weight HPMA-based polymers were higher compared with the high-molecular-weight counterpart. We assume that this is the result of the lower accessibility of phenolic groups in the interior of the polymer coils. Likewise, minor RCYs were observed for the lauryl methacrylate derivatives under the same conditions probably due to the formation of hydrophobic pockets leading to less-accessible tyramine moieties.

For biological experiments, the radiolabeled polymer systems were freed from low-molecular-weight byproducts using SEC leading to a pure, ^{18}F-labeled polymer solution ready for ex vivo and in vivo experiments in an overall synthesis of <90 min beginning at the start of [^{18}F]FETos synthesis.

Altogether, we were able to apply successfully the [^{18}F]fluoroethylation labeling method to a new series of HPMA homopolymers and HPMA-*ran*-LMA copolymers using optimized labeling conditions, thus enabling in vivo imaging of different polymeric architectures.

Table 3. Size of Homopolymers (P1*, P2*) and Random Copolymers (P3*, P4*) in Isotonic NaCl Solution by FCS at RT

nomenclature	concentration in mg/mL	R_h in nm	ΔR_h in nm
P1*	0.1	1.1	±0.1
P2*	0.1	3.0	±0.2
P3*	0.1	33.4	±1.7
P4*	0.1	39.9	±2.2

3.5. Biodistribution Studies. Figure 1A shows the impact of the molecular weight of the HPMA-homopolymers **^{18}F-P1*** and **^{18}F-P2*** on the biodistribution in different tissues ex vivo. The smaller polymer (**^{18}F-P1***, 12 kDa) showed highest concentrations in the kidneys (15.2 ± 3.1% ID/g tissue) and the liver (1.6 ± 0.1%ID/g tissue) 2 h after i.v. injection. These results correlate to already published data on the molecular weight dependence of HPMA copolymers,[45] ensuring that the nonbiodegradable HPMA-based polymer is cleared from the bloodstream by renal filtration if the molecular weight is low enough. In other organs, only marginal accumulation of the polymer was found.

In contrast, the high-molecular-weight homopolymer **^{18}F-P2*** (77 kDa) was found to be less pronounced in the kidneys (6.0 ± 0.1%ID/g tissue, Figure 1A), whereas in the liver the concentration was four times higher (8.0 ± 1.0%ID/g tissue), as compared with the **^{18}F-P1*** polymer. In addition, the accumulation in the spleen was also much higher (2.8 ± 0.2%ID/g tissue). These results indicate that the majority of i.v. injected radiolabeled high-molecular-weight polymer **^{18}F-P2*** cannot be filtered by the renal system and is presumably taken up by the macrophages of the MPS (mononuclear phagocyte system)[53] or is excreted by the liver and bile. This indicates that the molecular weight is an important factor for the route of elimination of well-defined polymeric architectures, as already demonstrated for ^{125}I-labeled HPMA copolymers by Seymour et al.[45] In comparison, the differences between the two polymers in other organs are

Table 4. Decay-Corrected Radiochemical Labeling Yields of Homopolymers (^{18}**F-P1*,** ^{18}**F-P2*) and Random Copolymers (**^{18}**F-P3*,** ^{18}**F-P4*) after 15 min at 120 °C Using 3 mg of Each Polymer Precursor in DMSO**

nomenclature	polymeric structure	monomer ratio[a]	M_w in g/mol[a]	RCY in %
^{18}F-P1*	homopolymer	100%	12.000	37 ± 6
^{18}F-P2*	homopolymer	100%	77.000	24 ± 2
^{18}F-P3*	random copolymer	82:18	14.000	26 ± 1
^{18}F-P4*	random copolymer	75:25	55.000	10 ± 2

[a] cf. Table 1.

Scheme 2. Radioactive Labeling of Homopolymers (P1*, P2*) and Random Copolymers (P3*, P4*) via Prosthetic Labeling Procedure Using [^{18}F]FETos

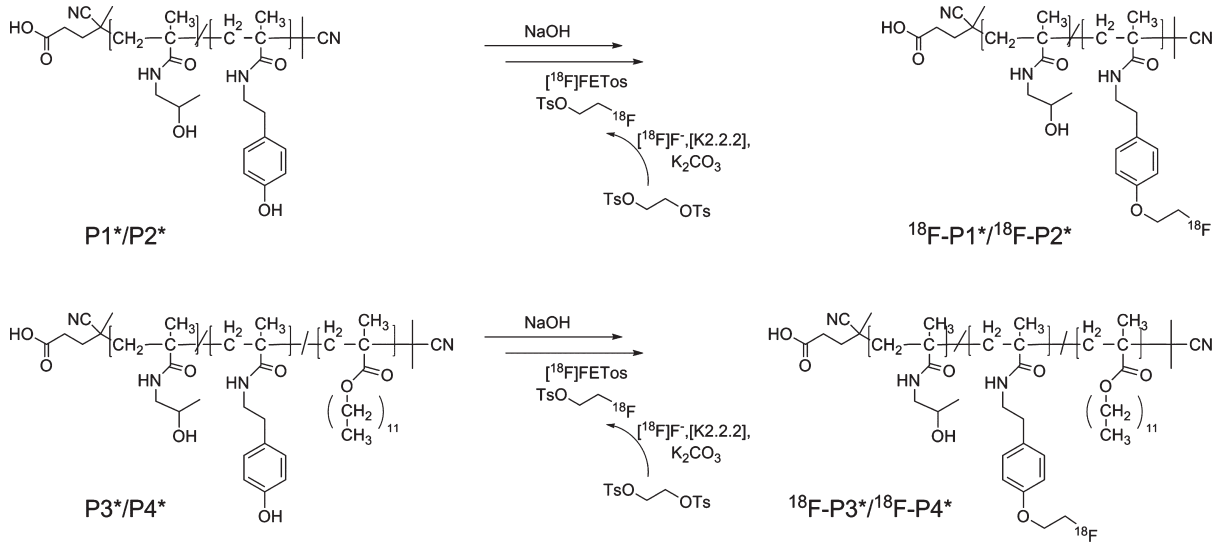

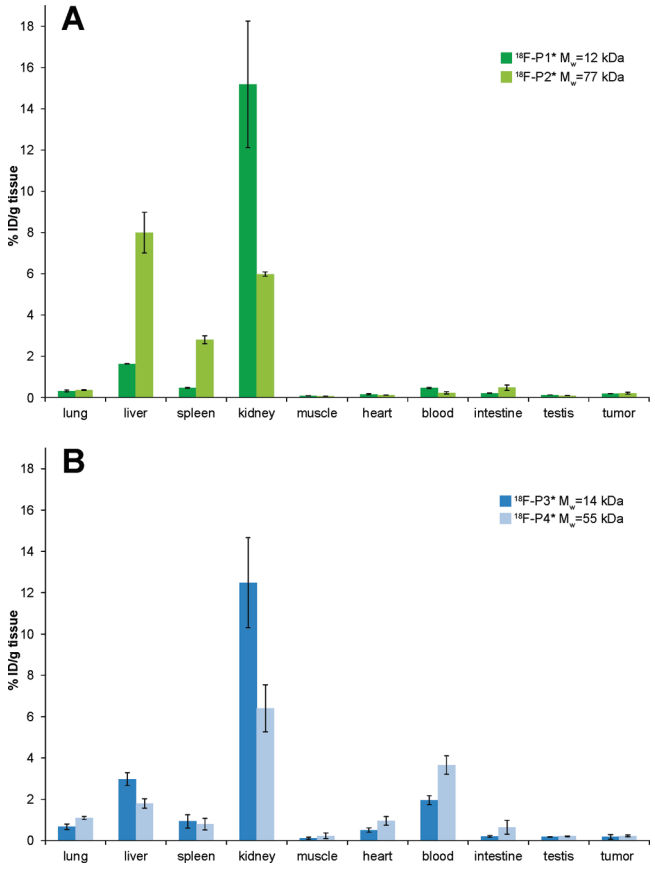

Figure 1. Influence of low- and high-molecular-weight HPMA-based homopolymers and random HPMA-LMA copolymers on their biodistribution in male Copenhagen rats bearing AT-1 R3327 Dunning prostate carcinoma 2 h post i.v. injection. (A) Recovered dose of injected **^{18}F-P1*** (M_w = 12 kDa) versus **^{18}F-P2*** (M_w = 77 kDa) in %ID/g tissue in organs of interest. (B) Recovered dose of molecular weight average 14 kDa (**^{18}F-P3***) and 55 kDa (**^{18}F-P4***) HPMA ran-LMA copolymers (n = 3).

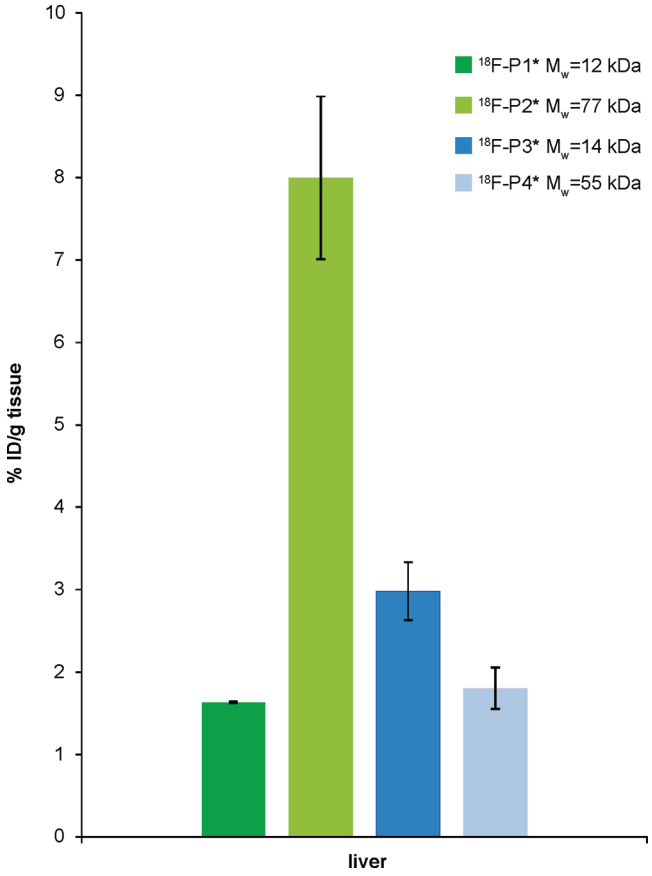

Figure 2. Liver uptake of **^{18}F-P1***—**^{18}F-P4*** in dependency of their molecular weight and polymer architecture 2 h p.i. expressed as %ID/g tissue.

marginal. In summary, most of the data received by the presented biodistribution study on HPMA-based homopolymers are comparable to the results of Lammers et al., who could demonstrate that different radioiodinated molecular weight poly(HPMA) showed significant disparities in body distribution.[39] Nevertheless, the polymers differed slightly in molecular weight, and the incorporation of the labeling group may also influence the in vivo behavior. By applying [^{18}F]fluoroethylation labeling, accumulation tendencies consistent with the above-mentioned results could be obtained, accomplished in a shorter time span and enabling the benefit of noninvasive high-resolution PET imaging, both favorable for patient selection concerning clinical therapies in the future.[19]

Similar experiments were performed with the well-defined HPMA-*ran*-LMA copolymers **^{18}F-P3*** and **^{18}F-P4***, which differed in molecular weight (14 kDa vs 55 kDa). These substances are different from the so-far studied HPMA-based copolymer systems for drug delivery[13,17,54] because the copolymerization of two methacrylate-based monomers (pentafluorophenyl and lauryl methacrylate) allows the preparation of randomly distributed copolymers. The incorporation efficiency of the hydrophobic fatty acid segment was calculated to be 18% for the low-molecular-weight copolymer **^{18}F-P3*** and 25% for the high-molecular-weight copolymer **^{18}F-P4***, respectively. When the body distribution of these probes was studied (Figure 1B), the low-molecular-weight polymer **^{18}F-P3*** was preferentially localized in kidney (12.6 ± 1.7%ID/g tissue), liver (3.0 ± 0.4%ID/g tissue), and blood (2.0 ± 0.3%ID/g tissue). In contrast, the high-molecular-weight polymer **^{18}F-P4*** showed higher levels in the blood (3.7 ± 0.5%ID/g tissue), and levels were lower in kidney (6.4 ± 1.2%ID/g tissue) and liver (1.8 ± 0.3%ID/g tissue). Both polymers were also found at low concentration in other organs such as lung, spleen, and heart (Figure 1B).

When comparing the corresponding polymers of the different types (homopolymer vs copolymer) of the approximately same sizes (**^{18}F-P1*** vs **^{18}F-P3*** and **^{18}F-P2*** vs **^{18}F-P4***), several pronounced differences can be seen. The most striking difference between the homo- and the copolymers is that independently from the molecular weight the HPMA-*ran*-LMA copolymer stays longer in the blood compartment. The small homopolymer was excreted rapidly by the kidneys and the large one by the liver, both leading to a negligible polymer concentration in the blood. The copolymers were excreted in the same principal manner, however, much slower, leading to marked sustained blood concentration. With an assumed blood volume of the rat of 16 mL,[50] the %ID/g blood values found for the copolymers translate into values of ~30% (**^{18}F-P3***) and 60% (**^{18}F-P4***) of the injected dose being still present in the blood compartment 2 h p.i., illustrating significant retention of the copolymeric systems in the bloodstream. In particular, the uptake of the larger copolymer **^{18}F-P4*** by the liver was much lower than that for the comparable homopolymer (as indicated by a four times lower accumulation in the liver, illustrated in Figure 2). Because the

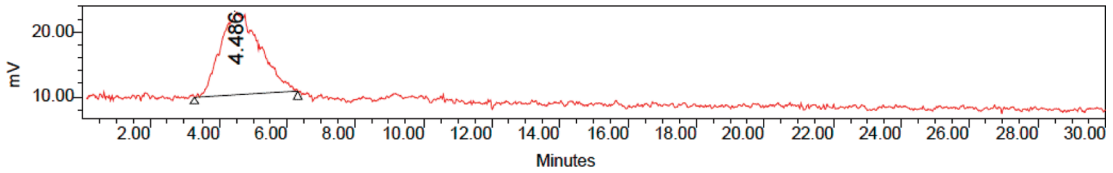

Figure 3. Sephadex G-25 chromatography of a blood plasma sample taken 140 min p.i. of the random copolymer **^{18}F-P4*** showing only one radioactive fraction of high molecular weight.

blood within the liver has not been washed out completely before taking the tissue samples, the measured signal might be slightly influenced by the tracer concentration in the blood. The question of specific liver uptake could be addressed in further experiments by using tracers with longer-lived isotopes for measuring late-stage accumulation after complete blood clearance.

In addition, the accumulation in the spleen (e.g., by uptake in macrophages) was less pronounced in the case of the copolymer **^{18}F-P4***. These results are indicating that the incorporation of the hydrophobic lauryl methacrylate segment holds a considerable impact on the biodistribution and especially on recognition mechanisms of the reticuloendothelial system (RES). By avoiding an increased uptake of the polymers by the cells of the MPS or by minimizing the renal filtration processes, the presence in the bloodstream can be significantly enhanced. The feature of a high long-lasting blood concentration is of high importance as a long-term uptake into a tumor or other organs of interest depends mainly on the plasma concentration of the drug.

Furthermore, it was tested whether ^{18}F-labeling of polymers cannot only be used for body distribution studies ex vivo but also for imaging and quantification of the compound's uptake into tumors. For this purpose, tumor-bearing rats (AT1) were used, and the tumor cell line was implanted subcutaneously on the hind food dorsum. The polymer was taken up into the tumor tissue, however, only to a very low amount. Despite the considerably higher concentration found for the copolymer systems in the blood pool 2 h p.i., no significant differences in tumor uptake was observed for all polymers tested. In fact, the concentration in tumor tissue was only marginally higher than that in the reference tissue (testis) in the field of view. Lammers et al.[39] reported for the same tumor model a much higher tumor uptake for large polymers (molecular weight 65 kDa) over a period of 168 h. Because in the present study only an observation period of 2 h was used (because of the short half-life of ^{18}F), the results are not directly comparable. Besides the fact that during 168 h AT1 tumors are markedly growing, which leads to a visual overestimation of polymer uptake in the images, the elimination (renal or liver/bile) of the polymer used by Lammers et al. seems to be much lower, resulting in a longer persistance of the polymer in the circulation. However, the uptake in the lung described by Lammers et al.[39] was not seen with any of the polymers in the present study (Figure 1) and cannot be explained at present.

3.6. Ex Vivo Blood Analysis. Using radiolabeling to trace polymeric architectures in vivo, metabolic stability of the radiolabel should be high. Loss of the radiolabel from the polymer due to radiolysis or enzymatic dehalogenation might lead to false estimation of accumulation patterns or to undesirable accumulation in sensitive tissues, as in the case of iodine which accumulates in the thyroid,[39,55] limiting diagnostic imaging, for example, with high gamma energy emitting ^{131}I. To study whether low-molecular-weight radioactive byproducts are present in the blood, blood samples were taken 140 min p.i., and blood plasma was analyzed

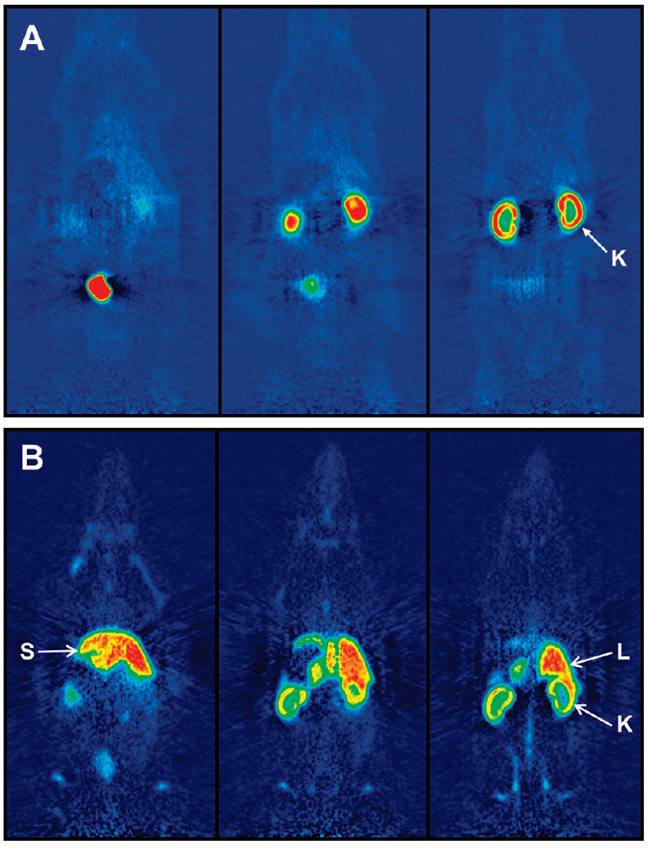

Figure 4. μPET imaging of ^{18}F-labeled homopolymers. Representative coronar μPET summed images in different depths 120−135 min after i.v. injection. (A) M_w = 12 kDa homopolymer **^{18}F-P1*** showing kidney elimination (K). (B) M_w= 77 kDa homopolymer **^{18}F-P2*** indicating accumulation in liver (L), spleen (S), and kidneys (K).

using SEC. As shown in Figure 3 for random copolymer, **^{18}F-P4*** the SEC chromatogram comprised only one radioactive fraction of high molecular weight, indicating that the radioactivity remains associated with the polymers over a time period of >2 h.

3.7. μPET Imaging. In addition to the biodistribution, differences in the pharmacokinetics of the various polymeric structures were visualized using μPET as noninvasive method with high spatial resolution. Therefore, dynamic PET images were obtained over 120 min after i.v. injection of the labeled polymers.

Representative whole body μPET images of both radiolabeled homopolymer systems of low and high molecular weight are shown in Figure 4. μPET images of low-molecular-weight homopolymer **^{18}F-P1*** (12 kDa) reveal that after 2 h almost the entire radioactivity localizes in kidneys and bladder (Figure 4A), whereas accumulation in other organs was barely visible. In correspondence with the biodistribution data obtained (Figure 1A), μPET

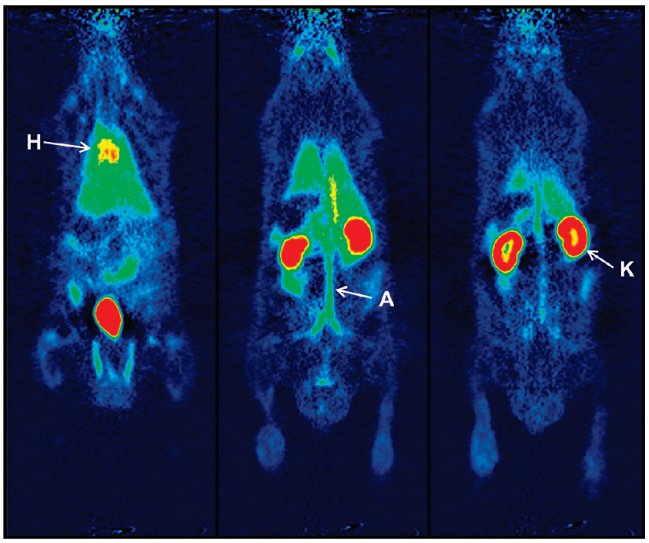

Figure 5. Representative coronar μPET images of HPMA-*ran*-LMA copolymer ^{18}**F-P4*** (55 kDa) 2 h after i.v. injection. The images show accumulation in kidneys (K) and bladder as well as remaining activity in the blood (heart (H); aorta (A)).

imaging of homopolymer ^{18}**F-P1*** precisely identifies a renal clearance, as expected for a hydrophilic polymeric system of 12 kDa being below the renal threshold for HPMA copolymers (M_w < 40 kDa).[45]

In contrast, whole-body μPET images of the high-molecular-weight homopolymer ^{18}**F-P2*** (77 kDa) demonstrate enrichment predominant in liver and spleen (Figure 4B), thereby again reflecting the findings of the biodistribution experiments. Despite the high molecular weight of 77 kDa (above the renal excretion threshold), small amounts of radioactivity can still be found in the kidneys, but excretion via the bladder was extremely slow. The μPET images obtained for ^{18}**F-P1*** and ^{18}**F-P2*** are demonstrated in Figure 4.

In contrast, imaging the distribution pattern of the large HPMA-*ran*-LMA copolymer ^{18}**F-P4*** in vivo, it clearly shows a reduced liver uptake (which is in good correspondence to the biodistribution experiments) (Figure 5) as compared with the large homopolymer (Figure 4B). Elimination of ^{18}**F-P4*** via the kidneys is comparable to the high-molecular-weight homopolymer ^{18}**F-P2***. In contrast to the homopolymer, the retention of the copolymer in the circulation (blood compartment) 2 h post injection is much higher (Figure 5, heart, aorta), already indicated by the biodistribution measurements.

4. CONCLUSIONS

In this study, we could demonstrate that the introduction of a radioactive probe allows systematic insight into the correlation between chemical structure and biodistribution of HPMA-based polymers of different M_w. In our case, we compared homopolymers versus random copolymers exhibiting lauryl methacrylate as hydrophobic segment. Because stability of the polymers could be ensured, the results emphasize the special benefit of introducing a radioactive label, in particular, when applying positron emission tomography, PET. It enables a precise tracing of the different polymer architectures in the organism and thereby gaining detailed knowledge about structure−property relationships of the polymers influencing their early phase organ accumulation.

The differing structures (**P1*** and **P2*** homopolymers vs. **P3*** and **P4*** random copolymers) had a major impact on the biodistribution pattern in the living organism. Our results differ from the results of Lammers[39] by the fact that the relative ratio of the accumulation in different tissue depends strongly on aggregate formation or not. In particular, the retention of the high M_w homopolymer and random copolymer is quite different. Despite a large superstructure formation of the HPMA-*ran*-LMA copolymers, renal clearance could still be proven, and liver accumulation was comparably low. Furthermore, the random copolymer P4* exhibited increased enrichment in the bloodstream (nearly 60% after 2 h p.i.), underlining its feasibility as model system for the design of amphiphilic transport vehicles for therapeutics in vivo. These results emphasize the significance of both (1) a good characterization of the polymers and their aggregates and (2) the use of in vivo pharmacokinetics, as it is available by PET, to evaluate the potential of biocompatible polymers as potential drug carriers.

■ ASSOCIATED CONTENT

Supporting Information. Experimental section-including polymer synthesis, FCS, and ring tensiometry setup, radioactive labeling, animal model and μPET setup. This material is available free of charge via the Internet at http://pubs.acs.org.

■ AUTHOR INFORMATION

Corresponding Author

*E-mail: zentel@uni-mainz.de. Tel: 0049-6131-39-20361.

Author Contributions

#Both authors contributed equally

■ ACKNOWLEDGMENT

We would like to thank Nicole Bausbacher, Bengü Yilmaz, and Hans-Georg Buchholz for their support during animal studies and following interpretation. Furthermore, we gratefully acknowledge Dr. Clemens K. Weiss and Elke Muth for their assistance during cmc determination measurements. We also want to thank the Max-Planck Graduate Center (MPGC, M. Allmeroth) as well as the Graduate School Materials Science in Mainz (Excellence Initiative, DFG/GSC 266, D. Moderegger) for financial support. In addition, we are very thankful for financial support of the DFG (Rösch: RO 985/30-1; Thews: TH 482/4-1, Zentel: ZE 230/21-1) and SAMT Initiative Mainz. We also thank Prof. Helmut Ringsdorf, Prof. Dr. Ruth Duncan, and Dr. Matthias Barz for stimulating discussions.

■ REFERENCES

(1) Duncan, R. *Nat. Rev. Drug Discovery* **2003**, *2*, 347–360.
(2) Matsumura, Y.; Maeda, H. *Jpn. J. Cancer Res.* **1986**, *46*, 6387–6392.
(3) Maeda, H.; Bharate, G. Y.; Daruwalla, J. *Eur. J. Pharm. Biopharm.* **2009**, *71*, 409–419.
(4) Ringsdorf, H. *J. Polym. Sci. Polym. Symp.* **1975**, *51*, 135–153.
(5) Obereigner, B.; Burešová, M.; Vrána, A.; Kopeček, J. *J. Polym. Sci., Polym. Symp.* **1979**, *66*, 41–52.
(6) Solovsky, M. V.; Ulbrich, K.; Kopecek, J. *Biomaterials* **1983**, *4*, 44–48.
(7) Duncan, R.; Seymour, L. W.; O'Hare, K. B.; Flanagan, P. A.; Wedge, S.; Hume, I. C.; Ulbrich, K.; Strohalm, J.; Subr, V.; Spreafico, F.;

Grandi, M.; Ripamonti, M.; Farao, M.; Suarato, A. *J. Controlled Release* **1992**, *19*, 331–346.
(8) Kopecek, J.; Kopecková, P.; Minko, T.; Lu, Z.-R. *Eur. J. Pharm. Biopharm.* **2000**, *50*, 61–81.
(9) Duncan, R. *Adv. Drug Delivery Rev.* **2009**, *61*, 1131–1148.
(10) Kataoka, K.; Harada, A.; Nagasaki, Y. *Adv. Drug Delivery Rev.* **2001**, *47*, 113–131.
(11) Gaucher, G.; Dufresne, M.-H.; Sant, V. P.; Kang, N.; Maysinger, D.; Leroux, J.-C. *J. Controlled Release* **2005**, *109*, 169–188.
(12) Barz, M.; Luxenhofer, R.; Zentel, R.; Kabanov, A. V. *Biomaterials* **2009**, *30*, 5682–5690.
(13) Talelli, M.; Rijcken, C. J. F.; van Nostrum, C. F.; Storm, G.; Hennink, W. E. *Adv. Drug Delivery Rev.* **2010**, *62*, 231–239.
(14) Duncan, R.; Gac-Breton, S.; Keane, R.; Musila, R.; Sat, Y. N.; Satchi, R.; Searle, F. *J. Controlled Release* **2001**, *74*, 135–146.
(15) Vicent, M. J.; Greco, F.; Nicholson, R. I.; Paul, A.; Griffiths, P. C.; Duncan, R. *Angew. Chem., Int. Ed.* **2005**, *44*, 4061–4066.
(16) Greco, F.; Vicent, M. J. *Adv. Drug Delivery Rev.* **2009**, *61*, 1203–1213.
(17) Duncan, R.; Vicent, M. J. *Adv. Drug Delivery Rev.* **2010**, *62*, 272–282.
(18) Lammers, T.; Subr, V.; Ulbrich, K.; Hennink, W. E.; Storm, G.; Kiessling, F. *Nano Today* **2010**, *5*, 197–212.
(19) Lammers, T.; Kiessling, F.; Hennink, W. E.; Storm, G. *Mol. Pharmaceutics* **2010**, *7*, 1899–1912.
(20) Herth, M. M.; Barz, M.; Moderegger, D.; Allmeroth, M.; Jahn, M.; Thews, O.; Zentel, R.; Rösch, F. *Biomacromolecules* **2009**, *10*, 1697–1703.
(21) Herth, M. M.; Barz, M.; Jahn, M.; Zentel, R.; Rösch, F. *Bioorg. Med. Chem. Lett.* **2010**, *20*, 5454–5458.
(22) Pimm, M. V.; Perkins, A. C.; Strohalm, J.; Ulbrich, K.; Duncan, R. *J. Drug Targeting* **1996**, *3*, 375–383.
(23) Mitra, A.; Nan, A.; Ghandehari, H.; McNeil, E.; Mulholland, J.; Line, B. *Pharm. Res.* **2004**, *21*, 1153–1159.
(24) Šprincl, L.; Exner, J.; Štďrba, O.; Kopeček, J. *J. Biomed. Mat. Res.* **1976**, *10*, 953–963.
(25) Minko, T.; Kopecková, P.; Pozharov, V.; Kopecek, J. *J. Controlled Release* **1998**, *54*, 223–233.
(26) Kopecek, J.; Kopecková, P. *Adv. Drug Delivery Rev.* **2010**, *62*, 122–149.
(27) Barz, M.; Luxenhofer, R.; Zentel, R.; Vicent, M. J. *Polym. Chem.* **2011**, DOI: 10.1039/C0PY00406E.
(28) Kopecek, J. *Polim. Med.* **1977**, *7*, 191–221.
(29) Kopecek, J.; Bazilová, H. *Eur. Polym. J.* **1973**, *9*, 7–14.
(30) Rathi, R. C.; Kopečková, P.; Říhová, B.; Kopeček, J. *J. Polym. Sci., Part A: Polym. Chem.* **1991**, *29*, 1895–1902.
(31) Ulbrich, K.; Subr, V.; Strohalm, J.; Plocová, D.; Jelínková, M.; Říhová, B. *J. Controlled Release* **2000**, *64*, 63–79.
(32) Seymour, L. W.; Duncan, R.; Strohalm, J.; Kopeček, J. *J. Biomed. Mater. Res.* **1987**, *21*, 1341–1358.
(33) Chiefari, J.; Chong, Y. K.; Ercole, F.; Krstina, J.; Jeffery, J.; Le, T.; Mayadunne, R.; Meijs, G.; Moad, C.; Moad, G.; Rizzardo, E.; Thang, S. H. *Macromolecules* **1998**, *31*, 5559–5562.
(34) Moad, G.; R., E.; Thang, S. H. *Aust. J. Chem.* **2005**, *58*, 379–410.
(35) Matyjaszewski, K.; Xia, J. *Chem. Rev.* **2001**, *101*, 2921–2990.
(36) Scales, C. W.; Vasilieva, Y. A.; Convertine, A. J.; Lowe, A. B.; McCormick, C. L. *Biomacromolecules* **2005**, *6*, 1846–1850.
(37) Gauthier, M. A.; Gibson, M. I.; Klok, H.-A. *Angew. Chem., Int. Ed.* **2009**, *48*, 48–58.
(38) Maeda, H.; Wu, J.; Sawa, T.; Matsumura, Y.; Hori, K. *J. Controlled Release* **2000**, *65*, 271–284.
(39) Lammers, T.; Kühnlein, R.; Kissel, M.; Subr, V.; Etrych, T.; Pola, R.; Pechar, M.; Ulbrich, K.; Storm, G.; Huber, P.; Peschke, P. *J. Controlled Release* **2005**, *110*, 103–118.
(40) Julyan, P. J.; Seymour, L. W.; Ferry, D. R.; Daryani, S.; Boivin, C. M.; Doran, J.; David, M.; Anderson, D.; Christodoulou, C.; Young, A. M.; Hesslewood, S.; Kerr, D. J. *J. Controlled Release* **1999**, *57*, 281–290.
(41) Seymour, L. W.; Ferry, D. R.; Kerr, D. J.; Rea, D.; Whitlock, M.; Poyner, R.; Boivin, C.; Hesslewood, S.; Twelves, C.; Blackie, R.; Schatzlein, A.; Jodrell, D.; Bissett, D.; Calvert, H.; Lind, M.; Robbins, A.; Burtles, S.; Duncan, R.; Cassidy, J. *Int. J. Oncol.* **2009**, *34*, 1629–1636.
(42) Hemmelmann, M.; Knoth, C.; Schmitt, U.; Allmeroth, M., Moderegger, D.; Barz, M.; Koynov, K.; Hiemke, C.; Rösch, F.; Zentel, R. *Macromol. Rapid Commun.* **2011**, DOI: 10.1002/marc.201000810C.
(43) Workman, P.; Twentyman, P.; Balkwill, F.; Balmain, A.; Chaplin, D.; Double, J.; Newell, D.; Raymond, R.; Stables, J.; Stephens, T.; Wallace, J. *Br. J. Cancer* **1998**, *77*, 1–10.
(44) Boyer, C.; Bulmus, V.; Davis, T. P.; Ladmiral, V.; Liu, J.; Perrier, S. *Chem. Rev.* **2009**, *109*, 5402–5436.
(45) Seymour, L. W.; Miyamoto, Y.; Maeda, H.; Brereton, M.; Strohalm, J.; Ulbrich, K.; Duncan, R. *Eur. J. Cancer* **1995**, *31*, 766–770.
(46) Eberhardt, M.; Mruk, R.; Zentel, R.; Theato, P. *Eur. Polym. J.* **2005**, *41*, 1569–1575.
(47) Theato, P. *J. Polym. Sci., Part A: Polym. Chem.* **2008**, *46*, 6677–6687.
(48) *Polymer Handbook*, 4th ed.; Brandrup, J., Immergut, E. H., Grulke, E. A., Abe, A., Bloch, D. R., Eds.; John Wiley & Sons: New York, 1999.
(49) Perrier, S.; Takolpuckdee, P.; Mars, C. A. *Macromolecules* **2005**, *38*, 2033–2036.
(50) Lee, H. B.; Blaufox, M. D. *J. Nucl. Med.* **1985**, *26*, 72–76.
(51) Yu, K.; Eisenberg, A. *Macromolecules* **1998**, *31*, 3509–3518.
(52) Trappmann, B.; Ludwig, K.; Radowski, M. R.; Shukla, A.; Mohr, A.; Rehage, H.; Böttcher, C.; Haag, R. *J. Am. Chem. Soc.* **2010**, *132*, 11119–11124.
(53) Owens Iii, D. E.; Peppas, N. A. *Int. J. Pharm.* **2006**, *307*, 93–102.
(54) Ulbrich, K.; Subr, V. *Adv. Drug Delivery Rev.* **2010**, *62*, 150–166.
(55) Wilbur, D. S. *Bioconjugate Chem.* **1992**, *3*, 433–470.